



MRI with TRELLIS: a novel approach to motion correction

Julian R. Maclaren, Philip J. Bones*, R.P. Millane, Richard Watts

Computational Imaging Group, Department of Electrical and Computer Engineering, University of Canterbury, Christchurch, New Zealand

Received 3 May 2007; revised 18 July 2007; accepted 8 August 2007

Abstract

A motion-correcting pulse sequence and reconstruction algorithm, termed TRELLIS, is presented. k -Space is filled using orthogonal overlapping strips and the directions for phase- and frequency-encoding are alternated such that the frequency-encode direction always runs lengthwise along each strip. The overlap between strips is used both for signal averaging and to produce a system of equations that, when solved, quantifies the rotational and translational motion of the object. Results obtained from simulations with computer-generated phantoms, a purpose-built moving phantom, and in human subjects show the method is effective. TRELLIS offers some advantages over existing techniques in that k -space is sampled uniformly and all acquired data are used for both motion detection and image reconstruction.

© 2008 Elsevier Inc. All rights reserved.

Keywords: MRI; FSE; Motion correction; Artifacts

1. Introduction

One disadvantage of MRI in comparison with other scanning modalities is the relatively long data acquisition time required. Thus, image quality is often degraded by motion artifacts, including image blurring and ghosting [1]. A number of techniques are employed to help ameliorate these problems: one is to prevent the motion occurring using sedation or physical restraints. Sedation involves risk [2] and also adds complication to the scan. Physically restraining patients is only partially effective. Navigator echo techniques have been used extensively and are becoming increasingly sophisticated [3–5] but still require the acquisition of extra data to determine motion. It is also possible to track subject motion using ultrasound [6], digital imaging [7], head-mounted tracking devices [8], or techniques such as using spectroscopy to identify the angle of rotation of a crystal containing deuterium [9]. An advantage of these techniques is that motion can be compensated for in real time by adjusting scanner gradients. However, the added complexity of these approaches is a significant disadvantage and none has yet achieved widespread clinical acceptance.

An alternative approach is to collect the data in such a way that the motion can be detected and corrected in post-processing. The advantage of this method is that no additional equipment is needed. One such technique that has achieved clinical success is PROPELLER MRI [10]. While PROPELLER has proved effective in reducing motion artifacts in both simulations [11] and clinical trials [12], it is slower than standard imaging sequences since the center of k -space is sampled multiple times [10]. Recent work combining EPI [13] and k -space under-sampling [14] with PROPELLER has produced promising results and may lead to faster implementations of PROPELLER in the future.

We have developed an alternative post-processing technique to correct for patient motion which we call ‘TRELLIS’ — an acronym for *Translation and Rotation Estimation using Linear Least-squares and Interleaved Strips* and so named because its sampling pattern looks like a trellis. This technique has some similarities to PROPELLER: it does not require extra hardware; it samples k -space more than once in order to obtain information about patient motion; and the final reconstruction requires some form of gridding. However, the data acquisition and image correction methods differ substantially and TRELLIS may offer significant advantages because the whole of k -space is uniformly sampled instead of concentrating sampling in the center of k -space as in PROPELLER.

* Corresponding author. Tel.: +64 3 364 2987x7275.

E-mail address: phil.bones@canterbury.ac.nz (P.J. Bones).

The purpose of this paper is to provide a full description of the TRELLIS k -space trajectory and reconstruction algorithm. Results from computer simulations, a physical ‘moving phantom’ and a human subject are presented. Through comparison with existing methods, the potential of TRELLIS as a clinical motion-correction technique is discussed.

2. Methods

TRELLIS data acquisition and reconstruction can be broken down into a number of consecutive steps. These are:

1. Data collection
2. k -Space alignment and centering
3. T_2 blurring correction
4. Motion detection
5. Motion correction
6. Gridding and final reconstruction.

These steps are described in the following subsections.

2.1. Data collection

The k -space trajectory used for TRELLIS is shown in Fig. 1. Samples are collected on a regular Cartesian grid in k -space within horizontal and vertical strips. In the example shown, the number of strips, N_s , is 16. Each strip consists of a number of lines (Fig. 1C), and the phase- and frequency-encode directions are selected so that the frequency encode direction is always parallel to these. The acquired data can be divided into two sets: H , k -space data acquired using horizontal strips; and V , k -space data acquired using vertical strips. Arrows in Fig. 1A and B indicate the phase-encode direction for each strip in H and V , respectively. The phase-encode direction is alternated between neighbouring strips to reduce discontinuities in k -space caused by T_2 decay (see T_2 blurring correction).

It is assumed that the acquisition time for each strip is small so that motion occurring while a strip is acquired is negligible. We have used fast spin echo (FSE) to ensure

that this assumption is satisfied in practice. The echo train length (ETL) then determines the number of lines within each strip. The order of acquisition used for the results presented here was all horizontal strips (left to right) followed by all vertical strips (top to bottom). However, this order is not important for image reconstruction. Strips can be interleaved (one horizontal strip, followed by one vertical strip, etc.), for example. The time interval between the acquisition of each consecutive strip is equal to the TR of the FSE sequence.

Imaging was performed using a 1.5 T Signa Excite HDx scanner (GE Medical Systems, Milwaukee, WI, USA) using a modified FSE sequence with matrix size 256×256 and NEX=1. Echo train lengths of both 16 and 32 were used successfully. For results shown in this paper, parameters were ETL=16, TR=2000 ms, slice thickness=10 mm (phantom) and ETL=32, TR=4520 ms, slice thickness=10 mm (human subject).

2.2. k -Space alignment and centering

The k -space data sets H and V , taken in their entirety, may be incorrectly centered (relative to the k -space origin) or misaligned (with respect to each other) due to eddy currents and other imperfections in the system such as slight differences between the gradients. They must therefore be aligned and centered for subsequent processing.

Misalignment between H and V manifests itself as a spatially varying phase difference between the two data sets after inverse transformation to image space, which leads to cancellation if the two complex data sets are combined (Fig. 2A). To align H and V in k -space, we extend the phase correlation method [15,16] to provide subpixel displacement information. First denote the inverse discrete Fourier transforms of H and V as \tilde{H} and \tilde{V} , respectively, defined in image space. The procedure, originally described by the authors in Ref. [17], is as follows:

1. Form a two-dimensional phase ramp function, $\Delta\varphi$, from the phase difference between \tilde{H} and \tilde{V} in image space.

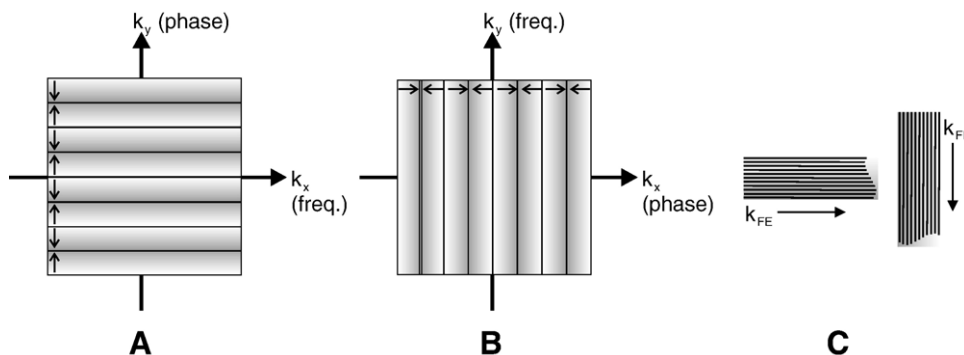


Fig. 1. TRELLIS data collection for $N_s=16$: (A) shows acquisition of eight horizontal strips forming the set H ; (B) shows acquisition of eight vertical strips, forming the set V . The phase-encode direction is indicated by arrows for each strip. Each strip comprises a number of lines as shown in (C), with the frequency-encode (FE) direction indicated.

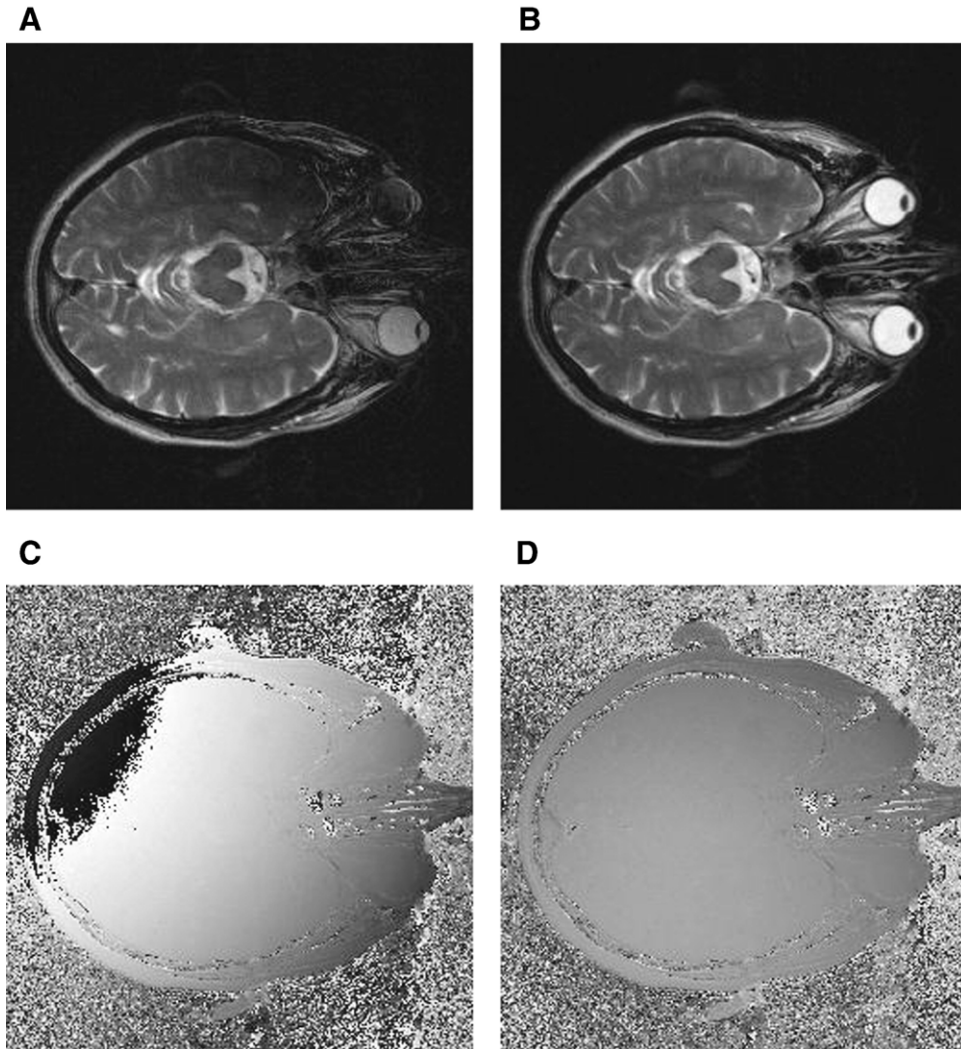


Fig. 2. Poor k -space alignment of H and V leads to cancellation in image space if the two data sets are combined (A). Correction by phase correlation gives the magnitude image in (B). However, a phase ramp in image space is still present (C); this results from the now-aligned H and V being incorrectly centered in k -space. After correction, the phase is that shown in (D).

2. Discrete Fourier transform the function $\exp(i\Delta\phi)$ and find the coordinates of the resulting maximum value in k -space. These provide an estimate of the gradient of $\Delta\phi$ and hence an estimate of the displacement between H and V in k -space.
3. In order to obtain subpixel accuracy, repeat Step 2. This time compute the DFT for values at and around the peak previously found in Step 2 in order to achieve a 100-fold increase in resolution of the peak location in k -space.
4. Add a phase ramp (with gradient found in Step 3) to \tilde{V} in image space and Fourier transform. This produces a new version of V , now aligned with H in k -space.

Once k -space alignment is complete (Fig. 2B), a constant phase offset between H and V may still exist. This is undesirable, as it is necessary to combine the two data sets later and any phase offset may result in signal cancellation.

To remove this offset, the phase distribution of all points in each data set H and V is computed. The difference between the peaks of the distributions corresponds to the phase offset between H and V . A constant phase is added to either H or V to correct for this.

Once H and V are aligned and have a similar phase, we use $S=H+V$ to determine the displacement of both H and V away from the k -space center. Experience has shown that prior alignment of H and V before k -space centering is more accurate than centering H and V individually. If S is not correctly centered in k -space, a phase ramp will be present in the image space function \tilde{S} (Fig. 2C). This is used to identify, and correct for, the displacement from the k -space origin in the same way as the displacement between H and V was found. It is also possible to locate the k -space center using a ‘center of mass’-type approach based on k -space magnitude; this alternative method appears to be equally effective.

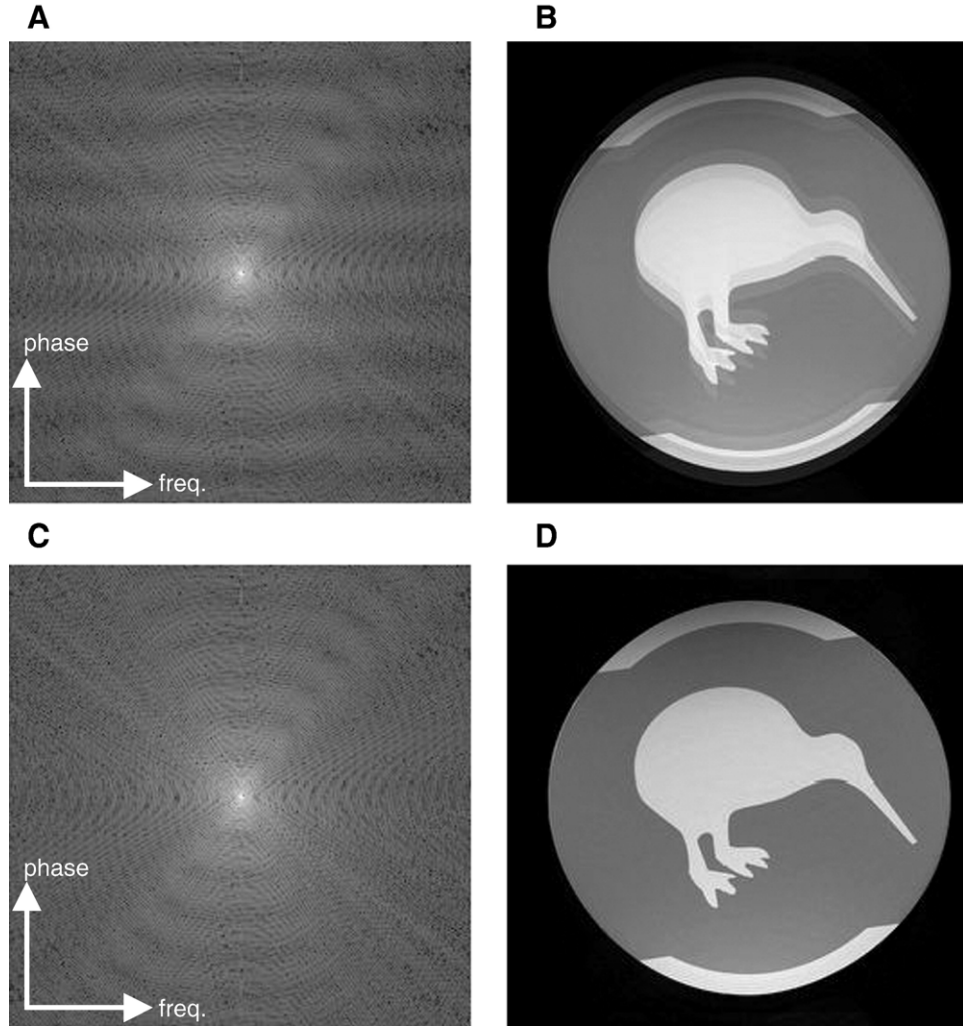


Fig. 3. Correction of H data using T_2 demodulation. Before correction: log k -space magnitude (A) and reconstructed image (B). After modulation correction: log k -space magnitude (C) and reconstructed image (D). Note the reduced blurring in the phase-encode direction in (D) compared to that in (B).

2.3. T_2 blurring correction

Signal amplitude decay due to T_2 effects causes a modulation of the k -space data. In turn, this produces blurring in the image in the direction corresponding to phase encoding. This problem is partly mitigated by reversing the order of acquisition of lines within neighbouring strips (Fig. 1A and B). However, some blurring remains. The effect of the modulation on k -space and image space (H and \tilde{H} data only) is shown in Fig. 3A and B for a stationary phantom filled with fluid having a relatively short T_2 . k -Space magnitudes are displayed using a log intensity scale for clarity. Note the blurring in the phase-encode direction in Fig. 3B.

The modulation function is estimated directly from the complete H and V data sets. To obtain $w(m)$, the modulation function in the phase-encode direction in the H data set, the magnitudes of both H and V k -space data sets are summed along their rows to form two vectors. Dividing the H vector by the V vector element-by-element yields a noisy estimate

of $w(m)$ (Fig. 4A). Denoting the number of frequency encode samples as N_{FE} and the number of lines acquired in the phase encode direction as N_{PE} , this procedure can be expressed as:

$$w(m) = \frac{\sum_{n=1}^{N_{FE}} |H(m, n)|}{\sum_{n=1}^{N_{FE}} |V(m, n)|}, \quad m = 1, 2, \dots, N_{PE}, \quad (1)$$

where (m, n) represents a data value in k -space, occupying the m th row and n th column.

As seen in Fig. 4A, the modulation function, $w(m)$, is approximately periodic with a period corresponding to the pairs of opposing strips. A smoother modulation function (Fig. 4B) is formed by combining the eight repeating sections in Fig. 4A to form an average and replicating this unit eight times to form an exactly periodic function. The H data are then corrected by normalizing each row of H using the modulation function (Fig. 3C and D). The same process

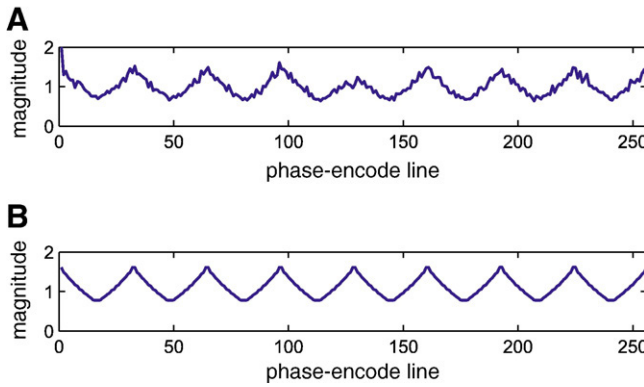


Fig. 4. The initial modulation function (A) as a function of k_{PE} computed for the data shown in Fig. 3. The eight repeating sections in (A) are averaged to form a single T_2 decay curve which is then replicated eight times along the length of k_{PE} to form the final smoothed periodic function (B). The vertical axis on each plot shows the relative magnitude of the k -space data plotted as a function of position in k -space in the phase-encode direction.

is used to correct V , but the initial summation is performed down each column rather than along each row.

Imperfections in the final image caused by T_2 signal decay still exist, particularly in the case of human subjects where T_2 values vary widely between different tissue types. However, the two steps described here greatly mitigate the effect.

2.4. Motion detection

The motion detection stage of the TRELLIS algorithm can be separated into two steps: rotation detection and translation detection. These two components are decoupled by using k -space magnitude to identify rotation and k -space phase for translation detection.

The rotational motion of the object during the scan can be identified by exploiting the rotation property of the two-dimensional Fourier transform. That is, if an object is rotated, the Fourier transform of that object is also rotated by the same angle, i.e.,

$$\begin{aligned} \tilde{G}(x, y) &\Leftrightarrow G(k_x, k_y) \\ \tilde{G}(x \cos \theta - y \sin \theta, x \sin \theta + y \cos \theta) &\Leftrightarrow G(k_x \cos \theta - k_y \sin \theta, k_x \sin \theta + k_y \cos \theta) \end{aligned} \quad (2)$$

where (x, y) is the location in image space, (k_x, k_y) is the location in k -space and \Leftrightarrow denotes two-dimensional Fourier transformation.

The rotation that has occurred between the measurement of two orthogonal strips can be determined by rotating one strip relative to the other to achieve the largest correlation between the k -space magnitudes in the overlapping region. An angular search width of $\pm 15^\circ$ with an increment of 0.1° was used.

The correlation is performed by transforming H and V into polar coordinates in k -space using spline interpolation of the real and imaginary parts. This is computationally efficient since interpolation only needs to be performed once

and testing individual rotation angles is reduced to a simple matrix shift.

There are $N_s/2$ vertical strips and $N_s/2$ horizontal strips resulting in $(N_s/2)^2$ overlapping sections, each giving a value, $\Delta\alpha_{mn}$, representing the relative angle between strips m and n . A linear system of equations can be formed and solved for the N_s-1 unknown rotation angles of each strip with respect to the first strip (defined arbitrarily as the reference).

Given the fitted rotation angles, each angle originally determined using correlation of strips can be compared to the fit and outliers excluded. When the erroneous measurements have been removed, the system of equations can be solved once more, yielding a result that is significantly more accurate than before. Outliers are identified by determining whether their measured value differs from the fitted value by more than a specified tolerance, ε_α . We have used $\varepsilon_\alpha=4^\circ$, determined empirically.

Once the absolute rotation angle of each strip in k -space has been determined, sections of data that overlap between strips are identified. In these overlapping sections, each sample is acquired twice: once as part of a vertical strip and once as part of a horizontal strip. If the object is unchanged, both samples will be identical; if the object has been translated by an amount $(\Delta x, \Delta y)$, the phase of the second sample will differ from the phase of the first sample by an amount proportional to $(\Delta x, \Delta y)$ and dependent on the location in k -space, (k_x, k_y) . This is a direct result of the Fourier shift theorem, i.e.,

$$\begin{aligned} \tilde{G}(x, y) &\Leftrightarrow G(k_x, k_y) \\ \tilde{G}(x - \Delta x, y - \Delta y) &\Leftrightarrow G(k_x, k_y)e^{j2\pi(k_x \Delta x + k_y \Delta y)}. \end{aligned} \quad (3)$$

The measured phase difference between matching points in strip m (horizontal) and strip n (vertical) within the region of overlap is given by

$$\Delta\phi_{mn} = (2\pi(k_x \Delta x_{mn} + k_y \Delta y_{mn}) + \text{noise}) \bmod 2\pi, \quad m, n \in 1, 2, \dots, N_s \text{ for } m \text{ even, } n \text{ odd}, \quad (4)$$

where N_s is assumed to be even. To complicate matters, phase can only be measured modulo- 2π as indicated in Eq. (4). Therefore the measured phase difference values must be unwrapped in order to determine Δx_{mn} and Δy_{mn} . To avoid the need for unwrapping, we again apply the phase correlation method described earlier (see k -Space alignment and centering), except that the k -space and image space roles are reversed, and use the measured phase ramp to directly give Δx_{mn} and Δy_{mn} .

In a manner similar to rotation detection, translation detection is applied to each pair of overlapping strips. This gives a set of values Δx_{mn} and Δy_{mn} , representing the translational shift in the object between the times at which strips m and n were acquired in the x - and y -directions, respectively. The procedure is then similar to the rotation detection stage. Again, there are $N_s/2$ horizontal strips and $N_s/2$ vertical strips, so there are $(N_s/2)^2$ equations in the form

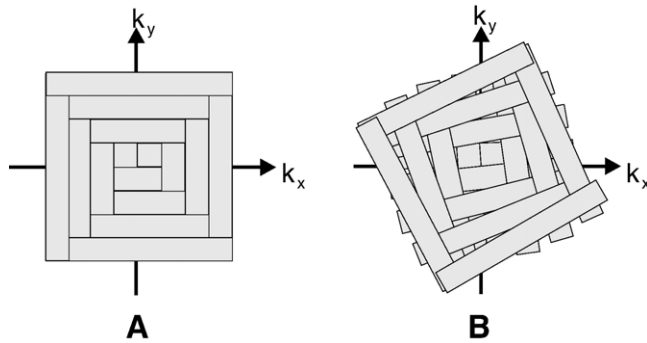


Fig. 5. Rotation correction in k -space. A depiction of the combined data sets H and V before rotation correction (A) and after correction (B). The position of the object during acquisition of each strip in k -space defines the frame of reference for that strip. Thus, k -space strips have been rotated and phase-adjusted individually so that these frames of reference are all aligned.

of Eq. (4). If the position of the object at the time Strip 1 is measured is taken to be the reference position, there are $N_s - 1$ pairs of unknowns: the $N_s - 1$ shifts of the object in image space as the sequence of strips is acquired. A system of equations linking relative displacements to absolute displacements is then formed and solved (as was done for rotation).

2.5. Motion correction

The rotation detection algorithm produces absolute rotation information for each strip in the H and V sets (i.e., an angle relative to a single reference strip rather than a large number of relative angles between all strips). These strips can then be rotated back by the same amount. The result of this procedure is illustrated in Fig. 5.

The translation detection algorithm gives the shifts in image space that occurred between the sampling of the first strip and each subsequent strip. Given this, the phase in each k -space strip can be adjusted, again using Eq. (4), to correct for the estimated motion.

2.6. Gridding and final reconstruction

Once all N_s strips in k -space have been rotated and phase-adjusted, they are gridded to the original Cartesian coordinate system using spline interpolation. This is straightforward because data points within each individual strip are still on a rectangular grid, i.e., interpolation is simply from one regular grid to another. Values obtained from different strips gridded to the same data point are averaged. Areas containing no data are filled using the Hermitian properties of k -space if possible, or left as zeros if not. We acknowledge that this is not a particularly sophisticated approach and other methods, such as reported in Ref. [18] or [19], may improve results. Lastly, the inverse discrete Fourier transform is applied to produce the final motion-corrected image.

3. Results

Testing has been performed in three stages: through simulations, using a moving phantom and with human subjects.

3.1. Simulations

Initially, the Shepp–Logan head phantom [20] has been utilised for testing purposes. It is widely used in medical imaging and is the sum of 10 ellipses of varying size and orientation. It is particularly convenient because its Fourier transform can be calculated analytically. Motion is simulated by separately computing each k -space strip. The position of the phantom is changed for each strip resulting in inconsistent k -space data which then leads to motion artifacts in the reconstruction.

The results of a simulation conducted to test the effectiveness of the TRELLIS algorithm are shown in Fig. 6. The simulated motion was a ‘random walk’ in both the horizontal and vertical directions and included rotation.



Fig. 6. Simulation results for a ‘random walk’ (exact parameters are shown in Fig. 7): image (A) shows the original Shepp–Logan head phantom; images (B) and (C) show uncorrected and corrected images, respectively, resulting from data acquisition during the period of simulated motion. The k -space data were corrupted to a level of 20 dB SNR.

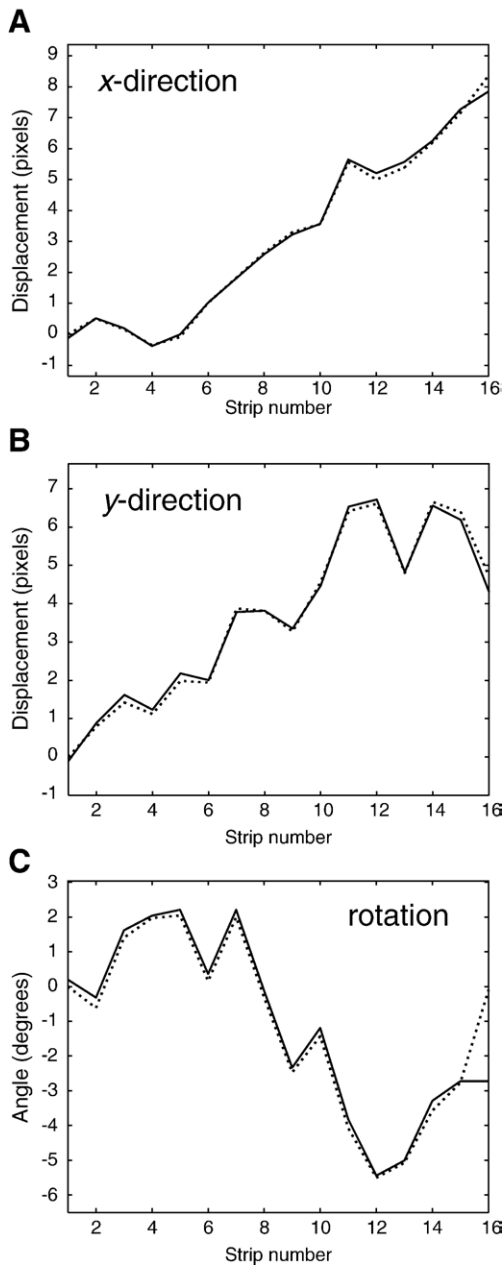


Fig. 7. Simulation results for a ‘random walk’ (cf. Fig. 6): detected motion for each strip (solid line) plotted together with actual motion simulated (dotted line). Displacement in the *x*-direction is shown in (A), displacement in the *y*-direction in (B) and rotation in (C). The mean errors between estimated and actual values are 0.10 pixels (A), 0.12 pixels (B) and 0.33° (C).

This was generated by shifting and rotating the object by a random amount between acquisition of each strip. The exact motion simulated is shown in Fig. 7. The number of strips used for the simulation, N_s , was 16. The image resolution was 256×256 pixels with a SNR of 20 dB (well below that found in most clinical images). SNR was calculated on the basis of signal ‘energy’, averaged over the entire field-of-view.

The motion parameters estimated by TRELLIS are shown together with the simulated motion in Fig. 7. This provides an estimate of the accuracy of the algorithm. The mean

difference between the actual and estimated displacement values in the *x*- and *y*-directions is 0.10 and 0.12 pixels, respectively. Rotation is detected with a mean error of 0.33° between actual and estimated angles for each strip. Mean error values were computed by averaging the absolute error between each corresponding actual (i.e., simulated) and measured displacement or rotation value.

Simulations indicate the corrected image is unaffected by the degree of motion occurring during the scan time, provided the phantom remains within the FOV. Thus the difference between the corrected and the uncorrected images becomes greater with increasing amounts of motion.

3.2. Moving phantom

In order to fairly compare the results of TRELLIS with a standard FSE acquisition, a moving phantom has been designed and built. The phantom was constructed using layers of polycarbonate glued together and then mounted inside an acrylic cylinder. Each layer was laser cut to achieve a precise result. The phantom was filled with water to generate a signal. In order to reduce T_1 and T_2 , 1.25 g/L CuSO₄·5H₂O (5 mmol) was added.

The phantom is moved using plastic pneumatic actuators, constructed from 60 mL syringes, to control translation and rotation. Air is fed to each syringe through 10 m of plastic pipe. This is sufficiently long to reach from the magnet room through a waveguide into the control room. Thus, there are no metallic components in the same room as the scanner.

A computer-controlled pneumatics system in the control room feeds air into the pipes and thus moves the phantom. The control unit consists of a programmable logic controller designed for real-time operation. This allows sequences to be tested with highly reproducible motion.

The phantom is shown in Fig. 8. Results obtained using it are shown in Fig. 9A–C. Fig. 9A shows the characteristic

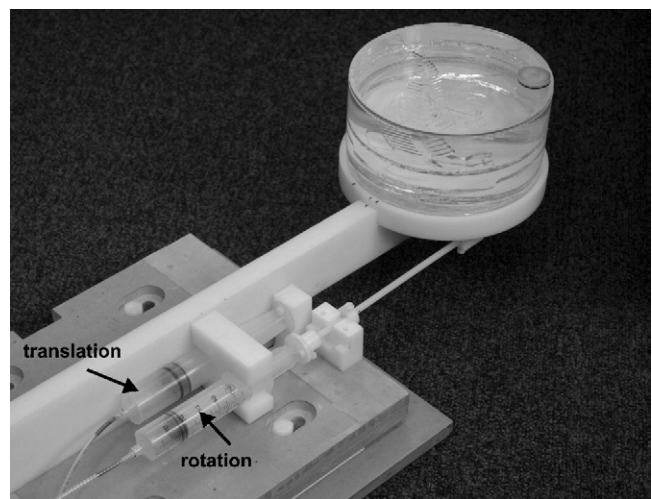


Fig. 8. The moving phantom. Rotation and/or translation (along a single axis only) is achieved using a pneumatics system. Air is fed to syringes which then move the platform holding the phantom.

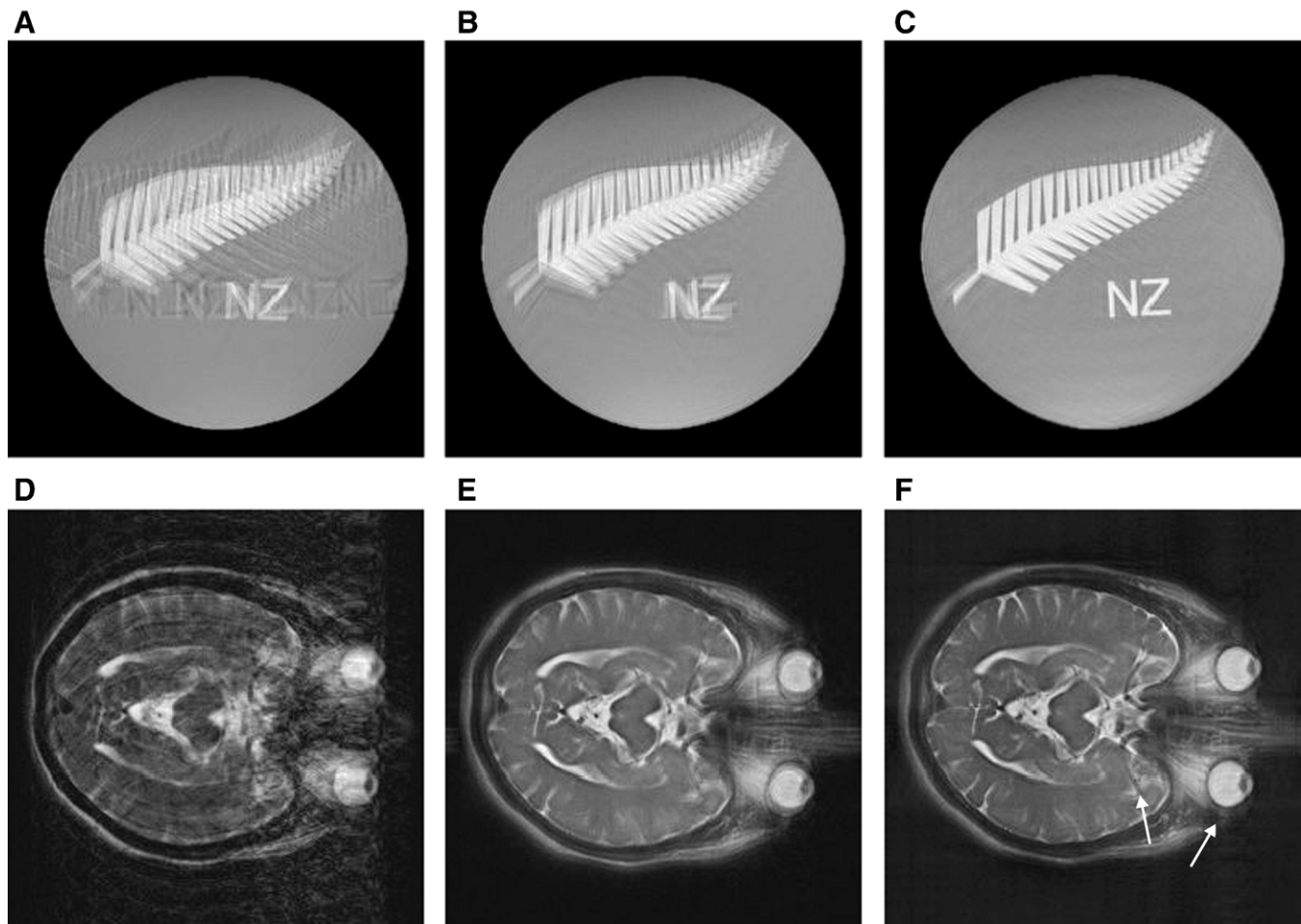


Fig. 9. Images obtained using standard interleaved FSE with an echo train length of 16 are shown in (A) and (D); images reconstructed using TRELLIS with motion correction disabled are given in (B) and (E); and images reconstructed using TRELLIS with motion correction are shown in (C) and (F). Arrows show the middle cerebral artery and the eye. Phantom motion used in (A)–(C) was a repeating rotation sequence (up to 15° in magnitude). The maximum motion detected by TRELLIS in (E) was a rotation of 3.8° and a translation of 1.6 pixels (*x*-direction) and 3.6 pixels (*y*-direction).

ghosting often seen with images obtained using a standard FSE sequence. The images in Fig. 9B (TRELLIS with no motion correction) and Fig. 9C (TRELLIS with motion correction) are significantly less motion-corrupted although the motion of the object was the same in all cases.

Although motion is reproducible to a high degree of accuracy, we have not yet developed a mechanism to measure the motion precisely during the scan and thus to directly determine the accuracy of TRELLIS. Work is progressing on a digital imaging-based approach to achieve this. In the meantime, however, the moving phantom serves to fairly compare the performance of different sequences when imaging a moving object. In some respects, this is a more robust test than imaging a moving human subject where motion is not repeatable.

3.3. Human subjects

Ethics approval was obtained for this study from the Upper South Ethics Committee, Christchurch, New Zealand.

Several normal, healthy volunteers were imaged using the TRELLIS sequence. Subjects were told to move their head in all directions throughout the scan and to try and make this motion as consistent as possible between scans. Thus, through-plane motion existed but was not corrected for, as would be the case in a clinical situation.

Typical results are shown for imaging using a standard FSE sequence (Fig. 9D), using TRELLIS without motion correction (Fig. 9E) and using TRELLIS with motion correction (Fig. 9F). The maximum motion detected was rotation of 3.8° and translation of 1.6 pixels (*x*-direction) and 3.6 pixels (*y*-direction). Due to the relative insensitivity to motion of the TRELLIS sequence, the differences between (E) and (F) are small. Note, however, the improved appearance of the middle cerebral artery and the eye in (F), as indicated by arrows.

In Fig. 9, image contrast differs between (D) and (E)–(F). This is due to different effective echo times (the time point at which the *k*-space center is

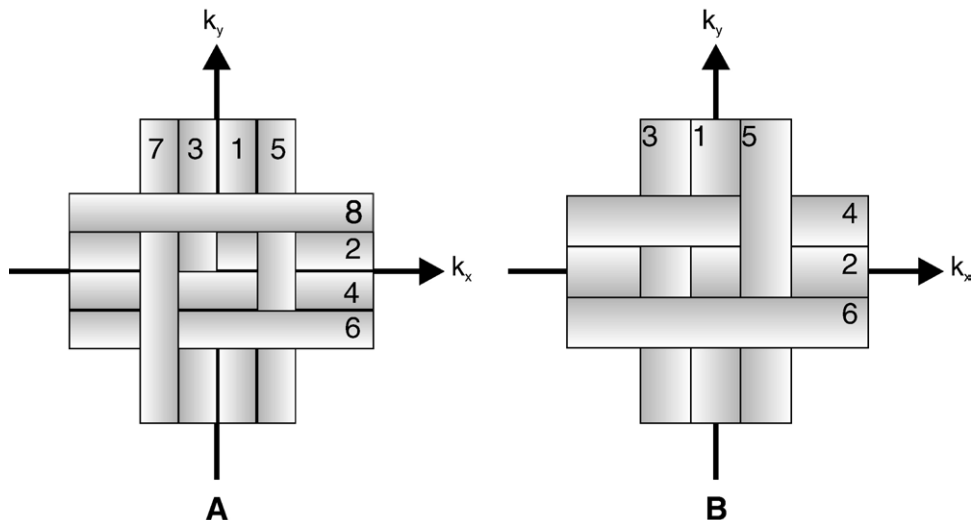


Fig. 10. Proposed future versions of TRELLIS for clinical use: TRELLIS with half the acquisition time (A); TRELLIS using an odd number of strips in H and V to maintain the integrity of the k -space origin (B). The numbering of each strip indicates one possible acquisition order.

sampled) between the FSE (102.7 ms) and the TRELLIS (6.4 ms) sequences.

4. Discussion

The newly proposed motion correction algorithm uses an interleaved acquisition of horizontal and vertical strips to fill k -space. This has several advantages over existing methods. All collected data are used for both motion correction and image reconstruction resulting in a more efficient (and hence more effective) algorithm. Unlike PROPELLER, the same acquisition time and SNR as a conventional algorithm (sampling twice then averaging) can be achieved. However, unlike a conventional algorithm, the acquired data can also be used to detect and correct for motion. Importantly, the sampling of k -space in TRELLIS is uniform. This means that the integrity of high spatial frequencies is more likely to be preserved when compared to PROPELLER, which samples the center of k -space much more densely than the outer regions. If a TRELLIS sequence is acquired in the absence of motion, the data acquired are very similar to that from a standard sequence. The only penalty in applying the method as a precaution against possible motion is some slight T_2 blurring resulting from imperfections in our demodulation approach as mentioned earlier (see T_2 blurring correction).

It could be assumed that data in the outer part of k -space are not useful for motion detection due to poor SNR. However, examination of TRELLIS results has shown this not to be the case. Although motion estimates from these areas are noticeably less reliable than those obtained by using data from the center of k -space, these estimates are still useful, particularly for rotation detection. This can probably be explained by the fact that a small rotation produces a significant displacement of data in the outer

regions, while the change may be too small to detect near the k -space origin.

It is interesting to note that the TRELLIS sequence is relatively robust to motion even without the application of motion correction performed in post-processing. This appears to be due to the damaging modulation of k -space that results from motion in standard interleaved sequences. Such modulation does not apply here; disruptions to k -space are inherently more gradual. In interleaved sequences, motion artifacts manifest themselves as ‘ghosts’ spread across the entire image. With a sampling scheme like TRELLIS, motion tends to result in blurring that is arguably less problematic in terms of image interpretation. The same effect has been observed with PROPELLER [12,21]. TRELLIS is, however, more susceptible to artifacts caused by T_2 decay.

It may be possible to implement TRELLIS using EPI or GRASE, as has been done with PROPELLER. EPI, however, is known for a high level of data warping and other artifacts; this could be problematic for TRELLIS. An obvious area of application for motion correction is in diffusion-weighted sequences. TRELLIS may have similar issues to other multishot diffusion-weighted sequences here, although aspects of the algorithm (such as the k -space centering stage) might aid in forcing consistency in k -space. Also encouraging is the fact that multishot diffusion-weighted FSE has been successfully implemented using PROPELLER [21].

A future development will be a version of TRELLIS that takes no longer than a standard FSE sequence with $\text{NEX}=1$ but can still accurately determine, and correct for, patient motion. This sequence, shown in Fig. 10A, has been successfully simulated but has not yet been implemented on the scanner. Simulations show that motion correction is at least as robust as the original TRELLIS sequence — not surprising as motion information is now derived from the central region of k -space where SNR is highest. The resolution in the final image is no longer isotropic as the

corners of k -space are not acquired. However, the visual appearance of images seems to be affected only slightly so, given the 50% reduction in acquisition time, this version of TRELLIS may be the one best suited for clinical use.

Another future modification may be the use of an odd number of strips, such that the first strip in H and V lies directly over the center of k -space (Fig. 10B). The advantage is that the center of k -space will always be kept intact, no matter what motion occurred during imaging. Currently, ‘holes’ in k -space near the origin caused by a gap between strips after rotation correction can occasionally cause artifacts. The optimum width of each strip has also yet to be found. Also note that TRELLIS has been demonstrated here using a square FOV but is equally applicable to a rectangular FOV: H and V do not need to contain the same number of strips.

Currently, no assumptions are made about the nature of the motion as a function of time. Incorporating prior knowledge of the maximum possible values of velocity or acceleration, for example, should further improve results. Likewise, the use of all slices in an acquired data set could greatly improve the robustness of the algorithm. As all slices are affected by motion with the same parameters, combining this motion information when correcting a single slice could be beneficial. It is anticipated that this extra information would be best included before solving the system of equations for rotation and translation. Instead of a single measurement of rotation between two strips, several measurements could be obtained. These could be averaged prior to solving the system of equations and the inverse variance between measurements used as a weighting function. A similar approach could be applied to PROPELLER.

5. Conclusion

The TRELLIS algorithm is unique in that it acquires data in a series of overlapping strips and then forms and solves a system of equations that link all motion information together. It offers an efficiency advantage over existing techniques such as PROPELLER, as all collected data are used for both motion detection and image reconstruction and excessive oversampling of the center of k -space is avoided. It is likely, however, that this advantage is gained at a cost of decreased motion detection accuracy compared to PROPELLER. Nevertheless, the accuracy of the TRELLIS algorithm is sufficient to enable accurate motion detection and it has proved effective at reducing motion artifacts for both a moving phantom and human subjects.

Acknowledgments

J. Maclarens is the recipient of a Top Achiever Doctoral Scholarship from the New Zealand Foundation for Research Science and Technology.

References

- [1] Liang Z-P, Lauterbur PC. Principles of magnetic resonance imaging: a signal processing perspective. New York: IEEE Press; 2000 [xv, 416 p.].
- [2] Malviya S, Voepel-Lewis T, Eldevik OP, Rockwell DT, Wong JH, Tait AR. Sedation and general anaesthesia in children undergoing MRI and CT: adverse events and outcomes. Br J Anaesth 2000;84(6):743–8.
- [3] Costa AF, Petrie DW, Yen YF, Drangova M. Using the axis of rotation of polar navigator echoes to rapidly measure 3D rigid-body motion. Magn Reson Med 2005;53(1):150–8.
- [4] Kadah YM, Abaza AA, Fahmy AS, Youssef ABM, Heberlein K, Hu XPP. Floating navigator echo (FNAV) for in-plane 2D translational motion estimation. Magn Reson Med 2004;51(2):403–7.
- [5] van der Kouwe AJW, Benner T, Dale AM. Real-time rigid body motion correction and shimming using cloverleaf navigators. Magn Reson Med 2006;56(5):1019–32.
- [6] Günther M, Feinberg DA. Ultrasound-guided MRI: preliminary results using a motion phantom. Magn Reson Med 2004;52(1):27–32.
- [7] Thesen S, Heid O, Mueller E, Schad LR. Prospective acquisition correction for head motion with image-based tracking for real-time fMRI. Magn Reson Med 2000;44(3):457–63.
- [8] Tremblay M, Tam F, Graham SJ. Retrospective coregistration of functional magnetic resonance imaging data using external monitoring. Magn Reson Med 2005;53(1):141–9.
- [9] Peshkovsky A, Knuth KH, Helpman JA. Motion correction in MRI using an apparatus for dynamic angular position tracking (ADAPT). Magn Reson Med 2003;49(1):138–43.
- [10] Pipe JG. Motion correction with PROPELLER MRI: application to head motion and free-breathing cardiac imaging. Magn Reson Med 1999;42(5):963–9.
- [11] Cheryauka AB, Lee JN, Samsonov AA, Defrise M, Gullberg GT. MRI diffusion tensor reconstruction with PROPELLER data acquisition. Magn Reson Imaging 2004;22(2):139–48.
- [12] Forbes KPN, Pipe JG, Bird CR, Heiserman JE. PROPELLER MRI: clinical testing of a novel technique for quantification and compensation of head motion. J Magn Reson Imaging 2001;14(3):215–22.
- [13] Skare S, Newbold RD, Clayton DB, Bammer R. Propeller EPI in the other direction. Magn Reson Med 2006;55(6):1298–307.
- [14] Arfanakis K, Tamhane AA, Pipe JG, Anastasio MA. k -Space undersampling in PROPELLER imaging. Magn Reson Med 2005;53(3):675–83.
- [15] Kuglin CD, Hines DC. The phase correlation image alignment method. In: Proceedings of the IEEE International Conference on Cybernetics and Society. New York: IEEE; 1975. p. 163–5.
- [16] Wu QX, Bones PJ, Bates RHT. Translational motion compensation for coronary angiogram sequences. IEEE Trans Med Imaging 1989;8(3):276–82.
- [17] Maclarens JR, Bones PJ, Millane RP, Watts R. Correcting motion artifacts in magnetic resonance images. In: McCane B, editor. Proceedings of Image and Vision Computing New Zealand. Dunedin, New Zealand: Image and Vision Computing New Zealand; 2005. p. 120–5.
- [18] Atkinson D, Hill DLG. Reconstruction after rotational motion. Magn Reson Med 2003;49:183–7.
- [19] Bammer R, Aksoy M, Liu C. Augmented generalized SENSE reconstruction to correct for rigid body motion. Magn Reson Med 2007;57(1):90–102.
- [20] Shepp LA, Logan BF. Fourier reconstruction of a head section. IEEE Trans Nucl Sci 1974;NS21(3):21–43.
- [21] Pipe JG, Farthing VG, Forbes KP. Multishot diffusion-weighted FSE using PROPELLER MRI. Magn Reson Med 2002;47(3):42–52.